HHS Public Access

Author manuscript

Nat Med. Author manuscript; available in PMC 2019 February 05.

Published in final edited form as:

Nat Med. 2017 November ; 23(11): 1277–1286. doi:10.1038/nm.4421.

Natural killer cells migrate into and control simian immunodeficiency virus replication in lymph node follicles in African green monkeys

Nicolas Huot[1,2], **Beatrice Jacquelin**[1], **Thalia Garcia-Tellez**[1], **Philippe Rascle**[1,3], **Mickaël J Ploquin**[1], **Yoann Madec**[4], **R Keith Reeves**[5], **Nathalie Derreudre-Bosquet**[6], and **Michaela Müller-Trutwin**[1,2]

[1]Unit on HIV, Inflammation and Persistence, Institut Pasteur, Paris, France.

[2]Vaccine Research Institute, Créteil, France.

[3]Université Paris Diderot, Sorbonne Paris Cité, Paris, France.

[4]Epidemiology Unit, Institut Pasteur, Paris, France.

[5]Center for Virology and Vaccine Research, Beth Israel Deaconess Medical Center, Harvard Medical School, Boston, Massachusetts, USA.

[6]Commissariat à l'Energie Atomique et aux Énergies Alternatives (CEA), Université Paris Sud 11, INSERM U1184, Immunology of Viral Infections and Autoimmune Diseases (IMVA), Institut de Biologie François Jacob (IBJF), Infectious Disease Models and Innovative Therapies (IDMIT) Department, Fontenay-aux-Roses, France.

Abstract

Natural killer (NK) cells play an essential role in antiviral immunity, but knowledge of their function in secondary lymphoid organs is incomplete. Lymph node follicles constitute a major viral reservoir during infections with HIV-1 and simian immunodeficiency virus of macaques (SIVmac). In contrast, during nonpathogenic infection with SIV from African green monkeys (SIVagm), follicles remain generally virus free. We show that NK cells in secondary lymphoid organs from chronically SIVagm-infected African green monkeys (AGMs) were frequently $CXCR5^+$ and entered and persisted in lymph node follicles throughout the follow-up (240 d post-infection). These follicles were strongly positive for IL-15, which was primarily presented in its membrane-bound form by follicular dendritic cells. NK cell depletion through treatment with anti-IL-15 monoclonal antibody during chronic SIVagm infection resulted in high viral replication rates in follicles and the T cell zone and increased viral DNA in lymph nodes. Our data suggest

Correspondence should be addressed to M.M.-T. (mmuller@pasteur.fr).

AUTHOR CONTRIBUTIONS

N.H. contributed to the project design, set up methods and performed the experiments; N.D.-B. provided samples; N.H., B.J., T.G.-T., P.R. and M.J.P. processed the samples; P.R. prepared the *IL15* probe; N.H. and Y.M. performed the statistical analyses; N.H., B.J., R.K.R. and M.M.-T. analyzed and interpreted the data; B.J. prepared the ethical protocols; N.H. and M.M.-T. wrote the manuscript; and M.M.-T. conceived the project and directed the research.

COMPETING FINANCIAL INTERESTS

The authors declare no competing financial interests.

Any Supplementary Information and Source Data files are available in the online version of the paper.

that, in nonpathogenic SIV infection, NK cells migrate into follicles and play a major role in viral reservoir control in lymph nodes.

The persistence of HIV in individuals effectively treated with combined antiretroviral therapy (cART) remains a tremendous obstacle to achieving sustained virologic remission in HIV-infected individuals[1]. Lymph nodes (LNs) are a major anatomical HIV reservoir[2,3]. Studies in the nonhuman primate model of HIV, macaques (*Macaca fascicularis*) infected with SIVmac, have shown that during the first weeks after infection the virus replicates solely in the T cell zone of LNs[4]. Only later on does the virus spread to B cell follicles, where it replicates to a large extent in follicular helper T (T_{FH}) cells[5–9]. Moreover, numerous viral particles are trapped by follicular dendritic cells (FDCs) and remain infectious for more than 9 months[10]. By contrast, in chronic infection, more virus is present in follicles than in the T cell zone[11,12]. In HIV controllers, the virus also persists preferentially in LN follicles, and productive infection is markedly restricted to T_{FH} cells[13]. LN B cell follicles thus seem to constitute ‘sanctuaries’ for persistent viral replication, even in HIV controllers who are capable of developing potent antiviral $CD8^+$ T cell responses[13]. Indeed, the B cell follicles are mostly devoid of $CD8^+$ T cells, except for rare follicular cytotoxic T cells[14]. T_{FH} cells also represent the major viral reservoir in patients under long-term cART, potentially complicating efforts to cure HIV infection with T cell immunotherapy[15,16].

NK cells play an essential role in viral infection[17,18]. However, little attention has been given to them in LNs, as their frequency is low in these tissues in contrast to other body compartments such as liver or uterus[19]. In rodent LNs, NK cells are denser in the medulla than in T or B cell areas, and they are mainly located within lymphatic sinuses[20,21]. Upon immunization or viral challenge, NK cells infiltrate draining LNs[22,23]. Little information is available regarding the trafficking of NK cells to LNs during viral infections in humans and on the migratory behavior of NK cells within LNs in general. During HIV-1 or SIVmac infection, LNs display limited recruitment of NK cells, which instead seem to be directed toward the intestinal mucosa, and therefore provide a niche in which the virus can replicate unabated by early NK cell–mediated innate pressure[24,25].

Nonhuman primates from Africa, such as AGMs (*Chlorocebus aethiops*), are natural hosts of SIV[25]. They usually do not experience disease progression, despite displaying high viremia and high viral replication rates in the intestine concomitant with massive acute depletion of mucosal $CD4^+$ T cells[26]. Major distinguishing features of SIV infection in natural hosts include the rapid resolution of viralinduced inflammation and the lack of microbial translocation[3,25]. In addition, AGMs display rapid control of viral replication in secondary lymphoid organs and a lack of viral trapping by FDCs in follicles[27–33]. Another natural host of SIV, the sooty mangabey (*Cercocebus atys*), also shows strong viral control in LNs[6,34].

In AGMs, most proinflammatory cytokines, such as tumor necrosis factor (TNF)-α, IL-6, interferon (IFN)-γ and IL-8, are not or are only weakly induced upon SIV infection[25]. However, AGMs display high plasma levels of IFN-α and IL-15 during acute infection[35]. IL-15 is well known to promote the mobilization and homeostatic proliferation of T cells and to be essential for the survival of NK cells[36,37]. Moreover, IL-15 contributes to the preservation of cytotoxic $CD8^+$ T cells and also enhances the suppressor function of NK

cells[38]. We have observed increases in NK cell proliferation as well as proliferation of CD107a$^+$ NK cells in peripheral LNs during acute SIVagm infection[35]. We therefore explored whether NK cells play a role in LNs during nonpathogenic SIV infection. Here we demonstrate that NK cells accumulate in an IL-15-dependent manner in the follicles of secondary lymphoid organs in SIV-infected AGMs and exert efficient control of viral replication within LNs, thus potentially contributing to a low viral reservoir in these organs.

RESULTS

Absence of virus in lymph node follicles in nonpathogenic SIV infection

We first determined the levels and distribution of virus in the LNs of six AGMs and six macaques infected with SIVagm.sab$_{92018}$ and SIVmac$_{251}$, respectively. The number of viral RNA copies in the plasma was always at least as high in AGMs as in macaques (Supplementary Fig. 1a–c). Peak viremia was reached around 9 days post-infection (d.p.i.) for all monkeys. Quantification of cell- associated viral RNA and DNA copy numbers in LN cells showed similarly high levels in SIVagm and SIVmac infections at peak viremia (Fig. 1a and Supplementary Fig. 1d). However, a strong decrease was observed after the viral peak in AGM LNs ($P = 0.001$). This viral control in AGM LNs resulted in a marked difference in virus levels in comparison to SIVmac infection, as the median quantities of cell-associated viral RNA and DNA in LNs were 2.5 and 1.5 log lower, respectively, in AGMs than in macaques during the chronic phase of infection (Fig. 1a and Supplementary Fig. 1d). Indeed, *in situ* evaluation of viral RNA showed dramatically lower numbers of productively infected cells in the T cell zone of AGM LNs during the chronic phase of infection and a persistent absence of productively infected cells within the follicles of AGM LNs throughout follow-up (to 240 d.p.i.) (Fig. 1b,c). These results contrast with those from SIVmac infection, in which, as expected, large amounts of viral RNA were detected both in the T cell zone and within follicles during chronic infection (Fig. 1b,c).

Accumulation of NK cells in lymph node follicles in nonpathogenic SIV infection

NK cells were gated as previously reported (Supplementary Fig. 2)[35,39]. A progressive and persistent reduction in the frequency of LN NK cells during chronic infection in comparison to preinfection levels ($P < 0.001$) was observed in the pathogenic model but not in AGMs, in which LN NK cells recovered to preinfection levels ($P = 0.8$) after a transient decline (Fig. 1d). The decrease observed in macaques was due to decline of the major NK cell population (i.e., CD16$^-$ NK cells) in LN, while, in accordance with a previous report in macaque LNs[39], there was an increase in the proportion of CD16$^+$ NK cells in SIVmac infection ($P < 0.001$) (Fig. 1g).

Evaluation of NK cell distribution *in situ* showed that NK cells in uninfected monkeys were localized, as expected, to the marginal and parafollicular zones of LNs in both species (Supplementary Fig. 3a). However, the localization of NK cells changed dramatically in response to SIV infection. Indeed, many NK cells were found outside of the marginal zone following SIV infection in both species (Supplementary Fig. 3b,c). Of note, the NK cell distributions in pathogenic and nonpathogenic SIV infections became highly distinct. In SIV-infected AGMs, NK cells were mostly found around or within follicles (Fig. 1e,f and

Supplementary Fig. 3b), whereas macaque NK cells followed a random distribution within the LN after SIV infection and did not accumulate in follicles (Fig. 1e,f and Supplementary Fig. 3c). Total numbers of NK cells decreased in the T cell zone in both species after SIV infection. In contrast to the macaque model, NK cell numbers increased in the follicles of AGMs (Fig. 1h).

These analyses reveal that the NK cell distribution within LNs changes considerably in response to SIV infection, and these changes are different in pathogenic and nonpathogenic infections. Moreover, study of nonpathogenic SIV infection demonstrates that NK cells are able to migrate into follicles.

Decreased lymph node homing receptors on NK cells in both pathogenic and nonpathogenic SIV infections

As macaques showed persistently decreased NK cell levels in LN as compared to AGMs, we asked whether AGM NK cells have greater LN homing capacity than NK cells in macaques during SIV infection. We examined the expression of major LN homing markers for NK cells (CCR7, CD62L, CX3CR1 and CXCR3). No changes in expression as compared to preinfection levels were detected in total peripheral blood NK cells in either species (Supplementary Fig. 4a,b), whereas $CD16^-$ NK cells displayed decreased CXCR3 and CX3CR1 expression in both species (Supplementary Fig. 5a,b).

In LN, the frequencies of NK cells expressing CCR7, CD62L or CX3CR1 were markedly downregulated in both pathogenic and nonpathogenic SIV infections (Supplementary Fig. 4). The decreases were again more pronounced in the $CD16^-$ subset than in the $CD16^+$ subset (Supplementary Fig. 5).

In sum, strong decreases in the expression of homing receptors were observed for both species, in particular for $CD16^-$ NK cells. The homing receptor profiles were similar for AGMs and macaques in most tissues and do not clearly explain the differences in LN NK cell levels between AGMs and macaques.

AGM NK cells express CXCR5 in secondary lymphoid organs in SIV infection

The preferential localization of NK cells in LN follicles during nonpathogenic SIV infection could be due to specific trafficking to follicles and/or to enhanced survival inside the follicles. To assess the possibility of specific trafficking, we measured the expression of CXCR5 on NK cells. CXCR5 is known to be both necessary and sufficient for B and T_{FH} cell migration into follicles[40,41]. We compared the levels of CXCR5 expression on B cells, $CD8^+$ T cells and NK cells in LNs from monkeys with chronic-phase infection (Fig. 2a). As expected, the majority of B cells expressed CXCR5, whereas a minority of $CD8^+$ T cells expressed it (Fig. 2a,b). The frequency of $CXCR5^+$ NK cells was also low among macaque NK cells but, surprisingly, was elevated in AGMs (Fig. 2a,b). In contrast to observations in spleen and LN, the levels of $CXCR5^+$ NK cells were similarly low in AGMs and macaques when assessed in blood and gut (jejunum and colon) (Fig. 2b).

Thus, we have identified high levels of CXCR5$^+$ NK cells in the LNs of SIVagm-infected AGMs. CXCR5 expression on AGM NK cells may allow their access to lymphoid tissue follicles.

Elevated frequencies of CD107a$^+$ and CD32$^+$CXCR5$^+$ NK cells in secondary lymphoid organs in nonpathogenic SIVagm infection

We asked whether these CXCR5$^+$ NK cells in the LN could have a suppressor function and characterized their functional phenotype (Fig. 2c–e). Major differences in expression of molecules associated with effector function were observed between CXCR5$^+$ and CXCR5$^-$ NK cells in the LNs of SIV-infected AGMs. Indeed, CXCR5$^+$ NK cells more frequently expressed CD69, CD16, CD107a and the Fcγ receptor CD32 than CXCR5$^-$ NK cells and more rarely expressed NKG2D and NKp46 (Fig. 2c–e). These cells might thus possess cytotoxic activity mediated by antibody dependent cell-mediated cytotoxicity (ADCC) and/or direct lysis. CXCR5$^+$ NK cells were more often positive for programmed death-1 (PD-1) than CXCR5$^-$ NK cells (Fig. 2d), which might be associated with their localization to follicles.

We wondered whether these results are representative of other secondary lymphoid organs and analyzed splenic NK cells from ten AGMs and ten macaques with chronic infection (Fig. 3). First, we quantified the cell-associated viral RNA and DNA loads in spleen. As in LN, they were significantly lower in AGMs than in macaques (Fig. 3a). Viral DNA levels were negatively correlated with NK cell levels in AGMs but not in macaques (Fig. 3c). As in LN, NK cell frequencies in spleen were higher in SIVagm than in SIVmac infection (Fig. 3d). The frequency of CXCR5$^+$ NK cells in spleen was again significantly higher in AGMs than in macaques, whereas CXCR5$^+$CD8$^+$ T cell frequencies were similar in the two species (Fig. 3b,e). The major phenotypic difference between splenic CXCR5$^+$ and CXCR5$^-$ NK cells consisted of higher frequencies of CXCR5$^+$ cells expressing CD107A and CD32 (Fig. 3f). Also in line with observations in LN, splenic CXCR5$^+$ NK cells were more often PD-1$^+$ and less often NKp46$^+$.

We then compared the NK cell phenotypes in AGMs and macaques in LN and spleen. As CXCR5$^+$ NK cells were rare in macaques, we used total NK cells in comparisons, the majority of which were CXCR5$^-$. No significant differences in the phenotypes of these cells were observed between AGMs and macaques, except that total NK cells in AGM spleens were more frequently CD32$^+$ than those in macaques; however, the difference in cell-surface expression was less than for CXCR5 and was not observed in LNs (Figs. 2e and 3g).

Taking these findings together, we observed elevated levels of CXCR5$^+$ NK cells expressing CD32 and CD107a in secondary lymphoid organs from SIVagm-infected AGMs.

AGM lymph node follicles constitute a niche for trans-presentation of IL-15

As NK cell numbers increased in follicles during SIVagm infection without these cells clearly showing a better homing receptor expression profile than in macaques, we wondered whether additional mechanisms, such as *in situ* proliferation or increased survival, contribute to the accumulation of NK cells in follicles during SIVagm infection. The levels of NK cell proliferation in LN, as measured by Ki-67 staining, were not higher during SIVagm infection

than during SIVmac infection (data not shown). Because IL-15 is essential for NK cell survival, we studied IL-15 production and distribution in the LN in response to SIV infection. We detected IL-15 in LN during infections with both viruses, but IL-15 production was significantly higher in AGMs than in macaques during chronic infection (Fig. 4a,b and Supplementary Fig. 6). In addition, IL-15 production was primarily limited to follicles, whereas in macaques it was diffuse (Fig. 4b and Supplementary Fig. 6). Remarkably, we observed NK cells in AGM follicles most often only if the follicles were IL-15^{+} (Fig. 4d).

To identify the cellular source of IL-15 in follicles, we examined the *ex vivo* expression of IL-15 in distinct hematopoietic and stromal cell subpopulations from the LNs of infected monkeys. Gating was performed in such a way as to allow the identification of as many as seven distinct cell populations (Supplementary Fig. 7a). We did not detect clear differences in IL-15 production by intracellular staining, even when the cells were stimulated with phorbol 12-myristate 13acetate (PMA) and ionomycin (data not shown). Thus, as intracellular analysis of IL-15 by flow cytometry was probably not sensitive enough to allow detection, we evaluated *in situ* expression of *IL15* mRNA by fluorescence *in situ* hybridization (FISH). Expression of *IL15* mRNA was higher in AGM LNs than in macaque LNs (Fig. 4e). Moreover, *IL15* mRNA was expressed predominantly within follicles during SIVagm infection. Many *IL15*-mRNA-positive cells had a dendritic-like shape and might thus correspond to FDCs or DCs located within the follicles.

IL-15 is particularly potent in stimulating immune responses if presented in its membrane-bound form. We therefore co-stained the hematopoietic and stromal cell subpopulations for cell-surface expression of IL-15 and the α subunit of its receptor, IL-15Rα (Supplementary Fig. 7). Most of the cells that presented membrane-bound IL-15 (mbIL15; i.e., IL-15^{+}IL-15Rα^{+} cells) corresponded to antigen-presenting cell (APC)-like cells (CD3^{-}CD4^{+}) and stromal cells, including FDCs. The most pronounced difference in the levels of mbIL-15 between AGMs and macaques was observed for FDCs (Fig. 4c).

We next addressed the question of whether distinct levels of IL15Rα in AGMs and macaques could explain these profiles. IL-15Rα expression was measured on the same cell populations as above. The percentages of IL-15Rα^{+} cells were highest for FDCs, whereas the mean intensities of expression were highest on APC-like cells (CD3^{-}CD4^{+}) and FDCs (Supplementary Fig. 7b,c). This was the case for AGMs. Thus, IL-15Rα expression levels are not responsible for the higher levels of mbIL-15 in AGMs.

In sum, NK cell accumulation in follicles during nonpathogenic SIVagm infection was associated with the presence of high levels of IL-15. IL-15 was produced within the follicles and presented in its membrane-bound form, in particular on FDCs.

Anti-IL-15 treatment of SIVagm-infected AGMs induces NK cell depletion

A major question is whether NK cells in AGM LNs have a crucial impact on viral load. We therefore aimed to deplete NK cells *in vivo* in AGMs. While there is presently no antibody specific for NK cells in primates, it has recently been reported that treatment with anti-IL-15 antibody preferentially and dramatically depletes NK cells in macaques[36]. We treated five

chronically infected AGMs with this anti-IL-15 monoclonal antibody using the same doses previously described for macaques for a short period of time (2 weeks) (Fig. 5a).

NK cells were rapidly depleted from the blood (Fig. 5b,c). The nadir in NK cell numbers was observed in three monkeys at day 7 after treatment and for two others at day 14. The latter two monkeys had higher levels of NK cells at baseline. The levels remained low until autopsy at day 42 post-treatment. In contrast, the percentages of $CD4^+$ T cells in total blood showed only a slight, transient increase ($P = 0.043$), and absolute $CD4^+$ T cell counts did not show any significant changes ($P = 0.21$) (Fig. 5d). The transient increases in $CD4^+$ T cell percentages might be explained by strong proliferation at days 7 and 14 (Fig. 5f). Blood $CD8^+$ T cell counts displayed a decrease that was mostly due to depletion of effector memory T cells (Fig. 5e).

Anti-IL-15 treatment depleted NK cells in all tissues analyzed, i.e., in LN, spleen and gut (Fig. 5b and Supplementary Fig. 8). In contrast to NK cells, the $CD4^+$ and $CD8^+$ T cell frequencies in LN were not different between day 0 and day 42 after treatment (Fig. 5g,h), with two exceptions. The frequencies of central memory $CD4^+$ T cells and effector memory $CD8^+$ T cells were decreased in LN at days 21 and 42 post-treatment (Fig. 5i,j).

Taking these findings together, we show that anti-IL-15 treatment results in marked depletion of NK cells in SIVagm-infected AGMs in blood and tissues, including LN.

NK cell depletion during SIVagm infection leads to high viral replication in lymph nodes

We quantified viral load in monkeys treated with anti-IL-15 anti-body. Viremia levels significantly increased after anti-IL-15 anti-body administration and reached a median plateau of around 10^5 viral RNA copies/ml at day 14 post-treatment (Fig. 6a). Notably, in LN, the amounts of cell-associated viral RNA and DNA were both significantly increased compared to untreated animals (Fig. 6b). *In situ* hybridization at days 21 and 42 post-treatment revealed many viral-RNA-positive cells in the LNs of all treated monkeys compared to uninfected animals (Fig. 6c), and large foci of viral-RNA-positive cells were detected in the T cell zone and within follicles. The increase in viremia in anti-IL-15-treated monkeys is most likely a result of this increase in viral replication in LNs. There was no statistically significant correlation between the levels of cell-associated viral RNA and DNA in LNs and the proliferation (measured by Ki-67) of total naive T cells, naive memory T cells or effector $CD8^+$ T cells in LNs.

To our knowledge, this is the first time that high numbers of SIV-infected cells have been observed within LN follicles in AGMs.

DISCUSSION

We present here the first documented evidence in any species, to our knowledge, of distinct anatomical localization within the LN of NK cells in response to lentiviral infection. Previous studies in mice have shown that infection with *Leishmania major* induces NK cell recruitment to the paracortex[20]. Similarly, we show that NK cells are recruited to the paracortex in response to SIV infection, but in addition we demonstrate that NK cells can

also accumulate around and within the follicles of peripheral LNs in SIV-infected AGMs. This is an important observation because it suggests that NK cells have the potential to interact directly with other cells present in LN follicles, such as B cells and T_{FH} cells. It has been shown in murine models that NK cells can influence T_{FH} and germinal center B cell responses[42–45]. Our results highlight the need for further studies of the effects of viral infections and vaccination on NK cell–B cell interactions and antibody responses and of the potential role of NK cell localization within follicles in mediating these responses.

In contrast to B and T cells, the mechanisms governing NK cell trafficking remain poorly dissected. In this study, we correlated the capacity of NK cells to migrate into follicles with CXCR5 expression. Moreover, we show that IL-15, an NK survival molecule, is found at high levels in the follicles of SIVagm-infected AGMs. IL-15 expression has recently been reported in the LNs of HIV-infected individuals, but only in the T cell zone[46]. We have shown that IL-15 is produced within follicles and presented in its membrane-bound form, in particular by FDCs, but also by APC-like cells, during SIVagm infection. This finding is in agreement with previous reports showing that human APCs and FDCs can present mbIL-15 (refs. 47,48). IL-15-mediated promotion of NK cell survival would then result in accumulation of these cells in a critical region of the LN. These results support previous reports suggesting the existence of *in situ*–differentiated NK cells in LN[39,49].

The effects of IL-15 on NK cell survival, differentiation and function are much stronger when IL-15 is presented *in trans* (i.e., membranebound), as is the case here, than when it is in its soluble form[50,51]. *In vitro* studies have indeed shown that the decreased control of HIV1 infection in $CD4^+$ T cells mediated by NK cells is due, at least *in vitro*, to decreased presentation of mbIL-15 (ref. 47). IL-15 induces lymphocyte function-associated antigen 1 (LFA-1) expression, which is a late step required for cytotoxic differentiation[52] of NK cells. Thus, in addition to promoting NK cell survival, the IL-15 in AGM follicles might contribute to differentiation toward a mature cytotoxic phenotype[53]. Our study reveals that many $CXCR5^+$ NK cells express CD107a, and even more $CXCR5^+$ NK cells express the Fcγ receptors CD16 and CD32. These NK cells might thus display superior ADCC. This notion needs to be confirmed by functional studies. Taking these findings together, $CXCR5^+$ NK cells clearly showed a distinct phenotype that could explain their superior capacity for viral control.

We confirm here strong viral control in LN during SIVagm infection. We cannot exclude the possibility that only follicles from peripheral secondary lymphoid organs are virus free. It is still possible that lymphoid structures in the gut allow viral replication and/or trapping, as viral replication is not controlled in the gut in natural hosts. We also cannot exclude the possibility that in AGMs the viral control in LN is stronger than that in other natural hosts, such as sooty mangabeys. However, our data are in line with previous reports of strong control of SIV infection in sooty mangabeys (SIVsm) in both the T cell zone and follicles of LNs[6,34]. HIV infection in LN causes inflammation that, when untreated, leads to collagen deposition, fibrosis and disruption of the LN architecture[10]. In addition, persistent HIV infection in LN might severely impact the development of effective immune cells[54,55]. Our results highlight the extraordinary capacity of AGMs to mount tissue-specific viral control. Our data, together with other studies showing that fewer memory $CD4^+$ T cells are infected

in natural hosts than in SIVmac-infected macaques and humans infected with HIV-1[3], suggest that natural hosts, although unable to control viremia, have developed mechanisms to specifically protect the organs and cells that are critical for the initial tailoring and subsequent memory of immune responses and to prevent viral-induced damage to secondary lymphoid structures. In addition, strong control of viral replication in secondary lymphoid organs might contribute to the lack of inflammation during chronic infection in natural hosts.

NK cell depletion during SIVagm infection was associated with strong increases in viral replication in the LN. This confirms the key role of NK cells in viral control in the LN. The increase in viral replication was observed both in the T cell zone and within follicles. It is unclear which NK cell phenotype is associated with viral control in the T cell zone. It is possible that in AGMs, in contrast to macaques, NK cells are not exhausted, as AGMs are capable of resolving chronic inflammation[25,39]. We also cannot totally exclude the possibility that in anti-IL-15-treated monkeys increases in $CD4^+$ target cells or decreases in $CD8^+$ T effector cells or their functions contributed to the greater viral load. However, in LN, the levels of memory $CD4^+$ T cells were either decreased or unchanged. With respect to $CD8^+$ T cells, previous studies have shown that AGMs infected with SIVagm do not exhibit a strong capacity for $CD8^+$ T cell suppression or substantial infiltration of $CD8^+$ T cells into LN follicles[28,56,57]. In addition, *in vivo* depletion of $CD8^+$ T cells in SIVagm-infected AGMs has not led to strong increases in viral load[58,59]. It is still possible that $CD8^+$ T cells contribute to the control of viral load in the LN during SIVagm infection, but it is unlikely that they play a major role in this model.

Genetic and functional studies have long highlighted the considerable impact of NK cells on HIV infection[18]. However, the role of NK cells in the control of HIV and SIV reservoirs might have been underestimated in the past. NK cells play an important role in immune surveillance in cancer. Clinical trials testing approaches to enhance NK cell expansion and suppressor activity in the context of cancer therapies are increasing. On the basis of our results, we anticipate that better comprehension of NK cell biology in lymphoid tissues, as provided here, will endorse the search for new NK cell–based immunotherapies for HIV infection.

Taken together, the results of this study reveal that SIV infection induces trafficking of NK cells within LNs. Most notably, we discovered unique CXCR5- and IL-15-dependent localization of NK cells within LN follicles. This study therefore uncovers a new feature of NK cells during viral infections. Furthermore, we provide evidence that NK cells have an unforeseen key role in nonpathogenic SIVagm infection in which they contribute to the control of viral replication in LNs. The discovery that NK cells have the potential to efficiently control the viral reservoir in LN follicles might have important implications for cure and vaccine research.

ONLINE METHODS

Monkeys, SIV infections and anti-IL-15 treatment.

Fifteen African green monkeys (Caribbean *Chlorocebus aethiops*) and 15 cynomolgus macaques (*Macaca fascicularis*) were used in this study. The monkeys were free of simian

retrovirus type D and simian T-lymphotropic virus type 1 and were housed in single cages within level 3 biosafety facilities at the IDMIT Center (Fontenay-aux-Roses, France). Because H6 haplotypes are notably associated with viral control in cynomolgus macaques, macaques with H6 haplotype were excluded from this study. The average weight of the monkeys was between 3 and 5 kg. All monkeys were young adults with an average age of 3–4 years at inclusion. Both males and females were used (60% females and 40% males for each species). The sample size varied between 5 and 10 monkeys per group ($n = 6$ in most experiments), chosen according to the tripartite harmonized International Council for Harmonization of Technical Requirements for Pharmaceuticals for Human Use (ICH) Guideline on Methodology (previously coded Q2B). Sample collection was performed in random order. The investigators were not blinded while the animal handlers were blinded to group allocation.

Monkeys were sedated with ketamine chlorhydrate (Rhone-Mérieux, Lyons, France) before handling. All experimental procedures were conducted in strict accordance with the international European guidelines 2010/63/UE on the protection of animals used for experimentation and other scientific purposes (French decree 2013–118) and with the recommendations of the Weatherall report. The IDMIT center complies with the Standards for Human Care and Use of the Office for Laboratory Animal Welfare (OLAW, USA) under OLAW Assurance number A5826–86. Monitoring of the monkeys was under the supervision of the veterinarians in charge of the animal facilities. Animal experimental protocols were approved by the Ethical Committee of Animal Experimentation (CETEA-DSV, IDF, France) (Notification 12–098). AGMs and macaques were infected intravenously with 250 median tissue culture infectious dose ($TCID_{50}$) of $SIVagm.sab_{92018}$ and 5,000 median animal infectious dose (AID_{50}) of $SIVmac_{251}$, respectively, as previously reported[28,35].

Of the six AGMs and six macaques described in Figure 1, four of each species were randomly chosen to be euthanized at 240 d.p.i., and the tissues (spleen and gut) used for the analyses described in Figures 2 and 3 were collected when the monkeys were euthanized. The spleens from the six additional monkeys described in Figure 3 correspond to randomly chosen, chronically $SIVagm.sab_{92018}$-infected AGMs from previous studies[35,60]. The two remaining AGMs from Figure 1 were included in the group of monkeys treated with simianized anti-IL-15 monoclonal antibody. The three other AGMs treated with anti-IL-15 monoclonal antibody derived from previous studies and were also randomly chosen[35]. The five AGMs were chronically infected with $SIVagm.sab_{92018}$ for 1–3 years at the time of anti-IL-15 administration.

Tissue collection and processing.

Blood and LN biopsies were collected longitudinally. Whole venous blood was collected in EDTA tubes. Mononuclear cells were isolated by Ficoll density-gradient centrifugation. Biopsies of peripheral LNs were performed by excision. Other tissues (spleen, gut) were collected at autopsy. After careful removal of adhering connective and fat tissues, LN and spleen were digested using collagenase IV, collagenase D and DNase I at 37 °C for 5 min. The tissue was then mechanically disrupted and filtered through a 40-μm cell strainer. Gut

was washed with cold medium and cut in pieces. A 20-min digestion with collagenase IV was performed at 37 °C. The cell suspension was filtrated subsequently through 100- and 40-μm cell strainers, and cells were washed with cold PBS. Cells were either immediately stained for flow cytometry or were cryopreserved in 90% FBS, 10% DMSO and stored in liquid nitrogen vapor.

Viral detection assays.

Plasma viral load was determined by real-time PCR as described[28]. For cell-associated viral RNA, RNA was extracted as follows: samples were lysed in NaCl (3 M), EDTA (0.5 M, pH 8), SDS (10%; Bio-Rad) and proteinase K (1 mg/ml; Qiagen) in a 45-min incubation at 55 °C. Then, NaCl (5 M) was added and samples were incubated at 4 °C between 15 and 60 min, followed by centrifugation for 15 min at 1,800*g* at 4 °C. DNA was precipitated in phenol:chloroform:isoamyl alcohol (25:24:1; pH 8; Sigma-Aldrich). Viral RNA was measured by qPCR in duplicate. SIVagm and SIVmac products of T7 transcription from plasmids were used as standards to calculate SIV RNA copy numbers. 18S ribosomal RNA and CCR5 DNA quantification were used for normalization. Sample preparation, enzyme mix preparation and PCR setup were performed in three separate rooms to avoid PCR contamination. Negative controls were used to exclude sample contamination.

Flow cytometry.

All analyses on blood cells and most analyses on LN cells, including those on the homing receptors, were performed on fresh cells. Hypotonic ammonium chloride solution was used to lyse contaminating red blood cells. Cytofix/Cytoperm (BD Biosciences, La Jolla, CA) was used for all intracellular staining. Intracellular staining for IL-15 was performed without and after stimulation with PMA and ionomycin at final concentrations of 10 ng/ml and 1 μg/ml, respectively. After 1 h of incubation, 10 μg/ml brefeldin A was added. FcR blocking reagent (Miltenyi) was used to block non-specific antibody binding. Antibodies used are shown in Supplementary Table 1. Flow cytometry acquisitions were done on an LSRFortessa (BD Biosciences), and FlowJo software (version 9.6.4, Tree Star, Ashland, OR) was used for all analyses.

Immunohistology.

Fresh LN tissues were embedded and snap frozen in optimum cold temperature compound (OCT), and 10-μm frozen sections were stained using unconjugated primary antibodies followed by appropriate secondary antibodies conjugated to Alexa Fluor 488 (green) or Alexa Fluor 568 (red) (Molecular Probes, Eugene, OR). Antibodies used are shown in Supplementary Table 2. NK cells were stained with NKG2A. Staining of NK cells was verified with other NK cell markers, such as NKp30 and NKp80 (data not shown). Stained slides were incubated with 100–200 μl of ice-cold methanol and 5% acetic acid, placed at −20 °C for 10 min and then washed. Image analysis was performed using a Leica TCS SP8 confocal microscope equipped with white lasers (Leica Microsystems, Exton, PA).

Fluorescent *in situ* hybridization.

Probes were prepared as follows. SIV *env* and *IL15* mRNA were amplified through RT–PCR, and cDNA was cloned using the CloneJET PCR Cloning Kit (Thermo Fisher Scientific), as recommended by the manufacturer. Vectors were digested and *in vitro* transcribed using T7 RNA polymerase (Ambion) to make Alexa Fluor 488 (Life Technologies) single-strand RNA probes. The FISH assay combined with immunofluorescent staining was performed as follows. Cryosections were rehydrated in PBS for 15 min and then permeabilized by incubation in 0.5% (v/v) Triton X-100 in PBS for 20 min at room temperature. The slides were placed in a container filled with 200 ml of 10 mM sodium citrate buffer (pH 6.0), and RNA was unmasked by putting the container in a microwave set at 700 W before heating for 2.5 min or until the first signs of boiling. This step was repeated seven times. The slides were transferred to 2× saline sodium citrate (SSC) and subsequently incubated in formamide–SSC solution for at least 4 h. The probe was mounted using glass chambers. Prehybridization was performed by incubating the slides with the mounted probe for 1–2 h at 37 °C. Cellular RNA and RNA probes were simultaneously denatured by incubating the slides with a mounted probe on a heating block for 5 min at 80 °C, followed by hybridization in humid dark chambers for 1 d at 37 °C. Sections were washed three times at high stringency in 0.1× SSC at 60 °C and three times in 2× SSC buffer. Finally, they were incubated in 0.05 μg/ml DAPI in SSC–Tween for 10 min, rinsed briefly in 2× SSC and mounted. As negative controls, we used a RNase-degraded probe, as well as LNs from uninfected monkeys. Images were acquired on a Leica TCS SP8 confocal laser scanning microscope, running LAS AF 3 (Leica Application Suite Advanced Fluorescence). Individual optical slices were collected at 1024 × 1024 pixel resolution. ImageJ software was used to assign colors to the channels collected.

Statistical analyses.

Nonparametric Mann–Whitney *U*-tests were used to compare continuous factors between two groups, and the nonparametric Wilcoxon signed-rank test was used to compare paired variables. The Spearman rank correlation was used to assess the association between two continuous variables. These statistical analyses, as well as graphic treatments, were performed with GraphPad Prism 7.0 software (GraphPad Software, La Jolla, CA). To evaluate changes over time, mixed-effects models were used to account for multiple repeated measurements, with testing of interactions between time and species; time was considered as a categorical or continuous variable depending on the number of values. We first assessed whether the marker's distribution was Gaussian; if not, a logarithmic transformation was used and tested if efficient. Second, a LOWESS (locally weighted scatterplot smoothing) curve was used to assess whether the marker's trajectory was linear. Finally, a mixed-effect linear or piecewise linear model was applied. Stata 13 (Stata Corp., College Station, TX, USA) was used for the analyses. In all analyses, $P < 0.05$ was considered significant.

Data availability.

Data from this study are available from the corresponding author upon reasonable request. A **Life Sciences Reporting Summary** is available.

Supplementary Material

Refer to Web version on PubMed Central for supplementary material.

ACKNOWLEDGMENTS

This work was supported by the Investissements d'Avenir program managed by the National Agency of Research (ANR) under reference ANR-10-LABX-77, the ANRS and the L'Oréal Foundation. The Infectious Disease Models and Innovative Therapies (IDMIT) center in Fontenay-aux-Roses, France, was funded by the French government's Investissements d'Avenir program for infrastructures (PIA) under grant ANR-11-INBS-0008, the PIA grant ANR-10-EQPX-02-01 funding the FlowCyTech facility at IDMIT. R.K.R. was supported by National Institutes of Health (NIH) grant RO1 DE026014. The anti-IL-15 monoclonal antibody was a gift from the NIH Nonhuman Primate Reagent Resource, supported by AI126683 and OD010976. N.H. and M.J.P. were recipients of postdoctoral fellowships from the French Vaccine Research Institute (Créteil, France) and Sidaction, respectively. P.R. and T.G.-T. received a PhD fellowship from the University Paris Diderot, Sorbonne Paris Cité (BIOSPC), and the Pasteur-Paris University PhD program supported by the Institut Carnot Pasteur Microbes et Santé, respectively. We are grateful to the veterinarians and the staff of the IDMIT animal facility, in particular V. Contreras, B. Delache, J.-M. Helies, V. Monnet, J. Morin and C. Joubert, for their excellent work. We thank L. Irbah, T. Kortulewski and C. Chapon for access to the stellar IDMIT imaging core facility as well as C. Cassan, S. Guenounou and A. Cosma for access to the state-of-the-art IDMIT FlowCyTech core facility.

References

1. Saez-Cirion A, Jacquelin B, Barré-Sinoussi F & Müller-Trutwin M Immune responses during spontaneous control of HIV and AIDS: what is the hope for a cure? Phil. Trans. R. Soc. Lond. B 369, 20130436 (2014). [PubMed: 24821922]
2. Lederman MM & Margolis L The lymph node in HIV pathogenesis. Semin. Immunol 20, 187–195 (2008). [PubMed: 18620868]
3. Paiardini M & Müller-Trutwin M HIV-associated chronic immune activation. Immunol. Rev 254, 78–101 (2013). [PubMed: 23772616]
4. Chakrabarti L et al. Early stages of simian immunodeficiency virus infection in lymph nodes. Evidence for high viral load and successive populations of target cells. Am. J. Pathol 144, 1226–1237 (1994). [PubMed: 8203463]
5. Lindqvist M et al. Expansion of HIV-specific T follicular helper cells in chronic HIV infection. J. Clin. Invest 122, 3271–3280 (2012). [PubMed: 22922259]
6. Brenchley JM et al. Differential infection patterns of $CD4^+$ T cells and lymphoid tissue viral burden distinguish progressive and nonprogressive lentiviral infections. Blood 120, 4172–4181 (2012). [PubMed: 22990012]
7. Petrovas C et al. CD4 T follicular helper cell dynamics during SIV infection. J. Clin. Invest 122, 3281–3294 (2012). [PubMed: 22922258]
8. Xu H et al. Persistent simian immunodeficiency virus infection drives differentiation, aberrant accumulation, and latent infection of germinal center follicular T helper cells. J. Virol 90, 1578–1587 (2015). [PubMed: 26608323]
9. Chowdhury A et al. Decreased T follicular regulatory cell/T follicular helper cell (TFH) in simian immunodeficiency virus–infected rhesus macaques may contribute to accumulation of T_{FH} in chronic infection. J. Immunol 195, 3237–3247 (2015). [PubMed: 26297764]
10. Estes JD Pathobiology of HIV/SIV-associated changes in secondary lymphoid tissues. Immunol. Rev 254, 65–77 (2013). [PubMed: 23772615]
11. Tenner-Racz K & Racz P Follicular dendritic cells initiate and maintain infection of the germinal centers by human immunodeficiency virus. Curr. Top. Microbiol. Immunol 201, 141–159 (1995). [PubMed: 7587348]
12. Fox CH et al. Lymphoid germinal centers are reservoirs of human immunodeficiency virus type 1 RNA. J. Infect. Dis 164, 1051–1057 (1991). [PubMed: 1955708]
13. Fukazawa Y et al. B cell follicle sanctuary permits persistent productive simian immunodeficiency virus infection in elite controllers. Nat. Med 21, 132–139 (2015). [PubMed: 25599132]

14. Leong YA et al. CXCR5^{+} follicular cytotoxic T cells control viral infection in B cell follicles. Nat. Immunol 17, 1187–1196 (2016). [PubMed: 27487330]
15. Banga R et al. PD-1^{+} and follicular helper T cells are responsible for persistent HIV-1 transcription in treated aviremic individuals. Nat. Med 22, 754–761 (2016). [PubMed: 27239760]
16. Miles B & Connick E T_{FH} in HIV latency and as sources of replication-competent virus. Trends Microbiol 24, 338–344 (2016). [PubMed: 26947191]
17. Vivier E, Tomasello E, Baratin M, Walzer T & Ugolini S Functions of natural killer cells. Nat. Immunol 9, 503–510 (2008). [PubMed: 18425107]
18. Carrington M & Alter G Innate immune control of HIV. Cold Spring Harb. Perspect. Med 2, a007070 (2012). [PubMed: 22762020]
19. Carrega P & Ferlazzo G Natural killer cell distribution and trafficking in human tissues. Front. Immunol 3, 347 (2012). [PubMed: 23230434]
20. Bajénoff M et al. Natural killer cell behavior in lymph nodes revealed by static and real-time imaging. J. Exp. Med 203, 619–631 (2006). [PubMed: 16505138]
21. Garrod KR, Wei SH, Parker I & Cahalan MD Natural killer cells actively patrol peripheral lymph nodes forming stable conjugates to eliminate MHC-mismatched targets. Proc. Natl. Acad. Sci. USA 104, 12081–12086 (2007). [PubMed: 17609379]
22. Beuneu H et al. Dynamic behavior of NK cells during activation in lymph nodes. Blood 114, 3227–3234 (2009). [PubMed: 19667398]
23. Sagoo P et al. *In vivo* imaging of inflammasome activation reveals a subcapsular macrophage burst response that mobilizes innate and adaptive immunity. Nat. Med 22, 64–71 (2016). [PubMed: 26692332]
24. Luteijn R et al. Early viral replication in lymph nodes provides HIV with a means by which to escape NK-cell-mediated control. Eur. J. Immunol 41, 2729–2740 (2011). [PubMed: 21630248]
25. Huot N, Rascle P, Garcia-Tellez T, Jacquelin B & Müller-Trutwin M Innate immune cell responses in non pathogenic versus pathogenic SIV infections. Curr. Opin. Virol 19, 37–44 (2016). [PubMed: 27447445]
26. Pandrea IV et al. Acute loss of intestinal CD4^{+} T cells is not predictive of simian immunodeficiency virus virulence. J. Immunol 179, 3035–3046 (2007). [PubMed: 17709518]
27. Beer B et al. Lack of dichotomy between virus load of peripheral blood and lymph nodes during long-term simian immunodeficiency virus infection of African green monkeys. Virology 219, 367–375 (1996). [PubMed: 8638402]
28. Diop OM et al. High levels of viral replication during primary simian immunodeficiency virus SIVagm infection are rapidly and strongly controlled in African green monkeys. J. Virol 74, 7538–7547 (2000). [PubMed: 10906207]
29. Gueye A et al. Viral load in tissues during the early and chronic phase of nonpathogenic SIVagm infection. J. Med. Primatol 33, 83–97 (2004). [PubMed: 15061721]
30. Goldstein S et al. Wide range of viral load in healthy African green monkeys naturally infected with simian immunodeficiency virus. J. Virol 74, 11744–11753 (2000). [PubMed: 11090174]
31. Broussard SR et al. Simian immunodeficiency virus replicates to high levels in naturally infected African green monkeys without inducing immunologic or neurologic disease. J. Virol 75, 2262–2275 (2001). [PubMed: 11160730]
32. Cumont M-C et al. Early divergence in lymphoid tissue apoptosis between pathogenic and nonpathogenic simian immunodeficiency virus infections of nonhuman primates. J. Virol 82, 1175–1184 (2008). [PubMed: 18032487]
33. Müller MC & Barré-Sinoussi F SIVagm: genetic and biological features associated with replication. Front. Biosci 8, d1170–d1185 (2003). [PubMed: 12957815]
34. Martinot AJ et al. Acute SIV infection in sooty mangabey monkeys is characterized by rapid virus clearance from lymph nodes and absence of productive infection in germinal centers. PLoS One 8, e57785 (2013). [PubMed: 23472105]
35. Jacquelin B et al. Innate immune responses and rapid control of inflammation in African green monkeys treated or not with interferon-α during primary SIVagm infection. PLoS Pathog 10, e1004241 (2014). [PubMed: 24991927]

36. DeGottardi MQ et al. Effect of anti-IL-15 administration on T cell and NK cell homeostasis in rhesus macaques. J. Immunol 197, 1183–1198 (2016). [PubMed: 27430715]
37. Cooper MA et al. *In vivo* evidence for a dependence on interleukin 15 for survival of natural killer cells. Blood 100, 3633–3638 (2002). [PubMed: 12393617]
38. Li J et al. Differential effects of IL-15 on the generation, maintenance and cytotoxic potential of adaptive cellular responses induced by DNA vaccination. Vaccine 33, 1188–1196 (2015). [PubMed: 25559187]
39. Schafer JL, Li H, Evans TI, Estes JD & Reeves RK Accumulation of cytotoxic $CD16^+$ NK cells in simian immunodeficiency virus–infected lymph nodes associated with *in situ* differentiation and functional anergy. J. Virol 89, 6887–6894 (2015). [PubMed: 25903330]
40. Gunn MD et al. A B-cell-homing chemokine made in lymphoid follicles activates Burkitt's lymphoma receptor-1. Nature 391, 799–803 (1998). [PubMed: 9486651]
41. Moser B, Schaerli P & Loetscher P $CXCR5^+$ T cells: follicular homing takes center stage in T-helper-cell responses. Trends Immunol 23, 250–254 (2002). [PubMed: 12102746]
42. Rydyznski C et al. Generation of cellular immune memory and B-cell immunity is impaired by natural killer cells. Nat. Commun 6, 6375 (2015). [PubMed: 25721802]
43. Abruzzo LV & Rowley DA Homeostasis of the antibody response: immunoregulation by NK cells. Science 222, 581–585 (1983). [PubMed: 6685343]
44. Blanca IR, Bere EW, Young HA & Ortaldo JR Human B cell activation by autologous NK cells is regulated by CD40–CD40 ligand interaction: role of memory B cells and $CD5^+$ B cells. J. Immunol 167, 6132–6139 (2001). [PubMed: 11714772]
45. Yuan D, Koh CY & Wilder JA Interactions between B lymphocytes and NK cells. FASEB J 8, 1012–1018 (1994). [PubMed: 7926365]
46. Younes S-A et al. IL-15 promotes activation and expansion of $CD8^+$ T cells in HIV-1 infection. J. Clin. Invest 126, 2745–2756 (2016). [PubMed: 27322062]
47. Moreno-Nieves UY, Didier C, Lévy Y, Barré-Sinoussi F & Scott-Algara D NK cells are primed by ANRS MVA_{HIV}-infected DCs, via a mechanism involving NKG2D and membrane-bound IL-15, to control HIV-1 infection in $CD4^+$ T cells. Eur. J. Immunol 44, 2370–2379 (2014). [PubMed: 24777763]
48. Park C-S, Yoon S-O, Armitage RJ & Choi YS Follicular dendritic cells produce IL-15 that enhances germinal center B cell proliferation in membrane-bound form. J. Immunol 173, 6676–6683 (2004). [PubMed: 15557159]
49. Freud AG et al. A human $CD34^+$ subset resides in lymph nodes and differentiates into $CD56^{bright}$ natural killer cells. Immunity 22, 295–304 (2005). [PubMed: 15780987]
50. Stonier SW & Schluns KS Trans-presentation: a novel mechanism regulating IL-15 delivery and responses. Immunol. Lett 127, 85–92 (2010). [PubMed: 19818367]
51. Tamzalit F et al. IL-15.IL-15Rα complex shedding following trans-presentation is essential for the survival of IL-15 responding NK and T cells. Proc. Natl. Acad. Sci. USA 111, 8565–8570 (2014). [PubMed: 24912180]
52. Barao I, Hudig D & Ascensao JL IL-15-mediated induction of LFA-1 is a late step required for cytotoxic differentiation of human NK cells from $CD34^+Lin^-$ bone marrow cells. J. Immunol 171, 683–690 (2003). [PubMed: 12847234]
53. Castillo EF, Stonier SW, Frasca L & Schluns KS Dendritic cells support the *in vivo* development and maintenance of NK cells via IL-15 trans-presentation. J. Immunol 183, 4948–4956 (2009). [PubMed: 19786554]
54. Onabajo OO & Mattapallil JJ Expansion or depletion of T follicular helper cells during HIV infection: consequences for B cell responses. Curr. HIV Res 11, 595–600 (2013). [PubMed: 24568615]
55. Racz P, Tenner-Racz K & Schmidt H Follicular dendritic cells in HIV-induced lymphadenopathy and AIDS. APMIS Suppl 8, 16–23 (1989). [PubMed: 2660879]
56. Zahn RC et al. Simian immunodeficiency virus (SIV)-specific $CD8^+$ T-cell responses in vervet African green monkeys chronically infected with SIVagm. J. Virol 82, 11577–11588 (2008). [PubMed: 18829748]

57. Lozano Reina J-M et al. Gag p27-specific B- and T-cell responses in simian immunodeficiency virus SIVagm-infected African green monkeys. J. Virol 83, 2770–2777 (2009). [PubMed: 19109377]

58. Schmitz JE et al. Inhibition of adaptive immune responses leads to a fatal clinical outcome in SIV-infected pigtailed macaques but not vervet African green monkeys. PLoS Pathog 5, e1000691 (2009). [PubMed: 20011508]

59. Gaufin T et al. Experimental depletion of CD8+ cells in acutely SIVagm-infected African green monkeys results in increased viral replication. Retrovirology 7, 42 (2010). [PubMed: 20459829]

60. Jacquelin B et al. Nonpathogenic SIV infection of African green monkeys induces a strong but rapidly controlled type I IFN response. J. Clin. Invest 119, 3544–3555 (2009). [PubMed: 19959873]

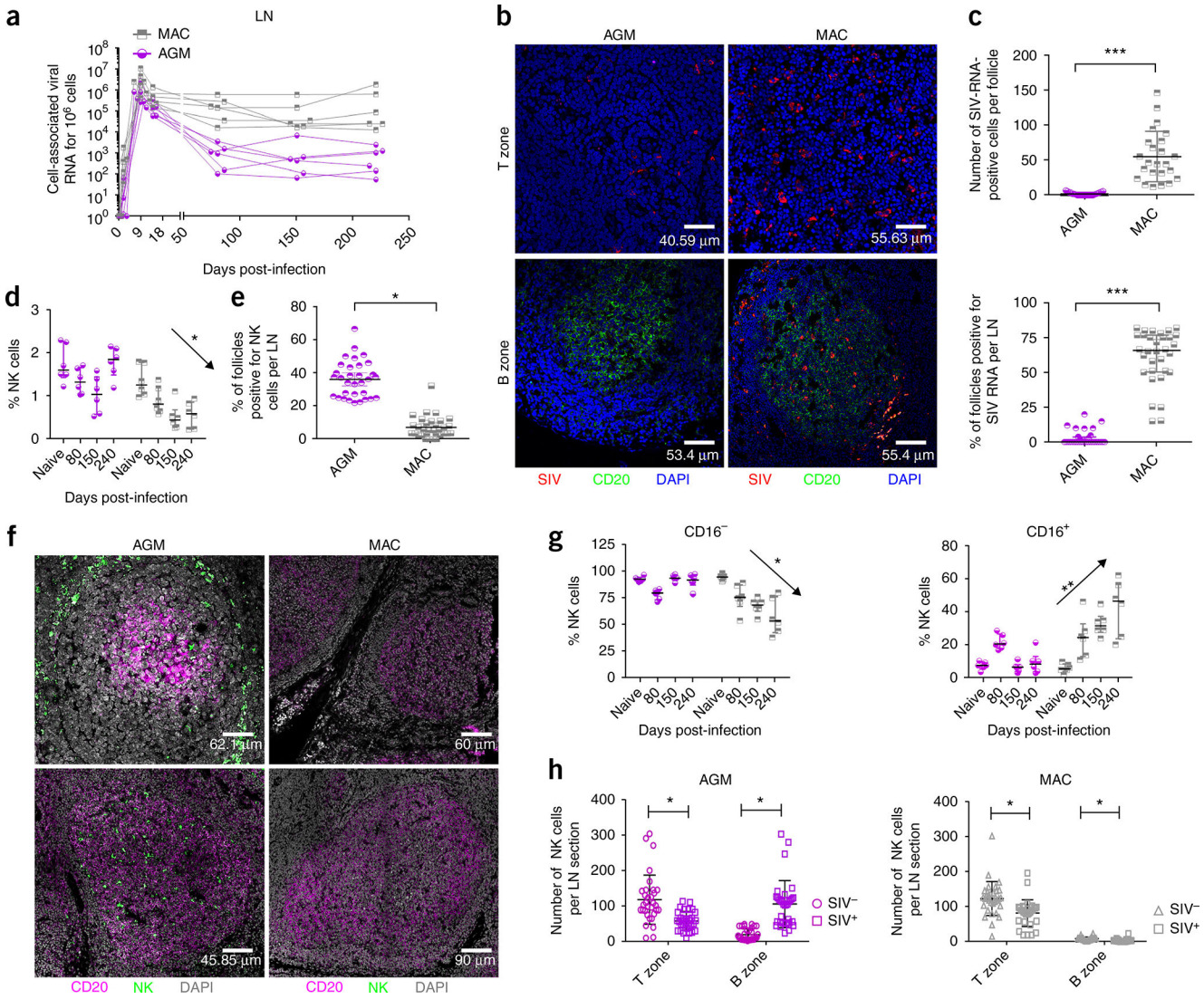

Figure 1.

Numbers and distribution of SIV RNA and NK cells in lymph nodes. Peripheral LNs from six AGMs and six macaques (MAC) infected with SIVagm and SIVmac, respectively, were analyzed. (**a**) Cell-associated viral RNA per 10^6 total LN cells. (**b**) Representative confocal images of LN sections from chronically infected monkeys stained for B cells (CD20, green), SIV RNA (red) and nuclear DNA (blue). Viral RNA was detected by *in situ* hybridization. Images present the distribution of productively infected cells in LN. One representative image each for the B and T cell zones is shown for each species. (**c**) Top, number of SIV-RNA-positive cells per follicle. A total of 24 follicles were counted. Bottom, number of follicles positive for SIV RNA. A total of eight LN sections per animal were counted. (**d**) Frequency of NK cells among total $CD45^+$ lymphocytes in the LNs of AGMs (purple) and macaques (gray). (**e**) Percentage of follicles positive for at least one NK cell. A total of 32 LN sections were counted. (**f**) Examples of the distribution of NK cells in LNs during chronic SIVmac and SIVagm infections as evaluated by confocal imaging. NK cells were stained with anti-NKG2A antibody (green), and B cells were stained with anti-CD20

antibody (purple). In AGMs, NK cells were observed around (upper left) or inside the follicles (bottom left). (**g**) Frequencies of $CD16^{-}$ and $CD16^{+}$ NK cells in LNs from AGMs (purple) and macaques (gray). (**h**) Numbers of NK cells in the T and B cell zones. A total of 32 LN sections from six monkeys per species were counted (4–6 sections per animal). For **c**, **e** and **h**, a nonparametric Mann–Whitney *U*-test was used for statistical analysis. For **d** and **g**, a mixed-effect model was used. $*P < 0.05$, $**P < 0.005$, $***P < 0.001$. Median and interquartile range are shown.

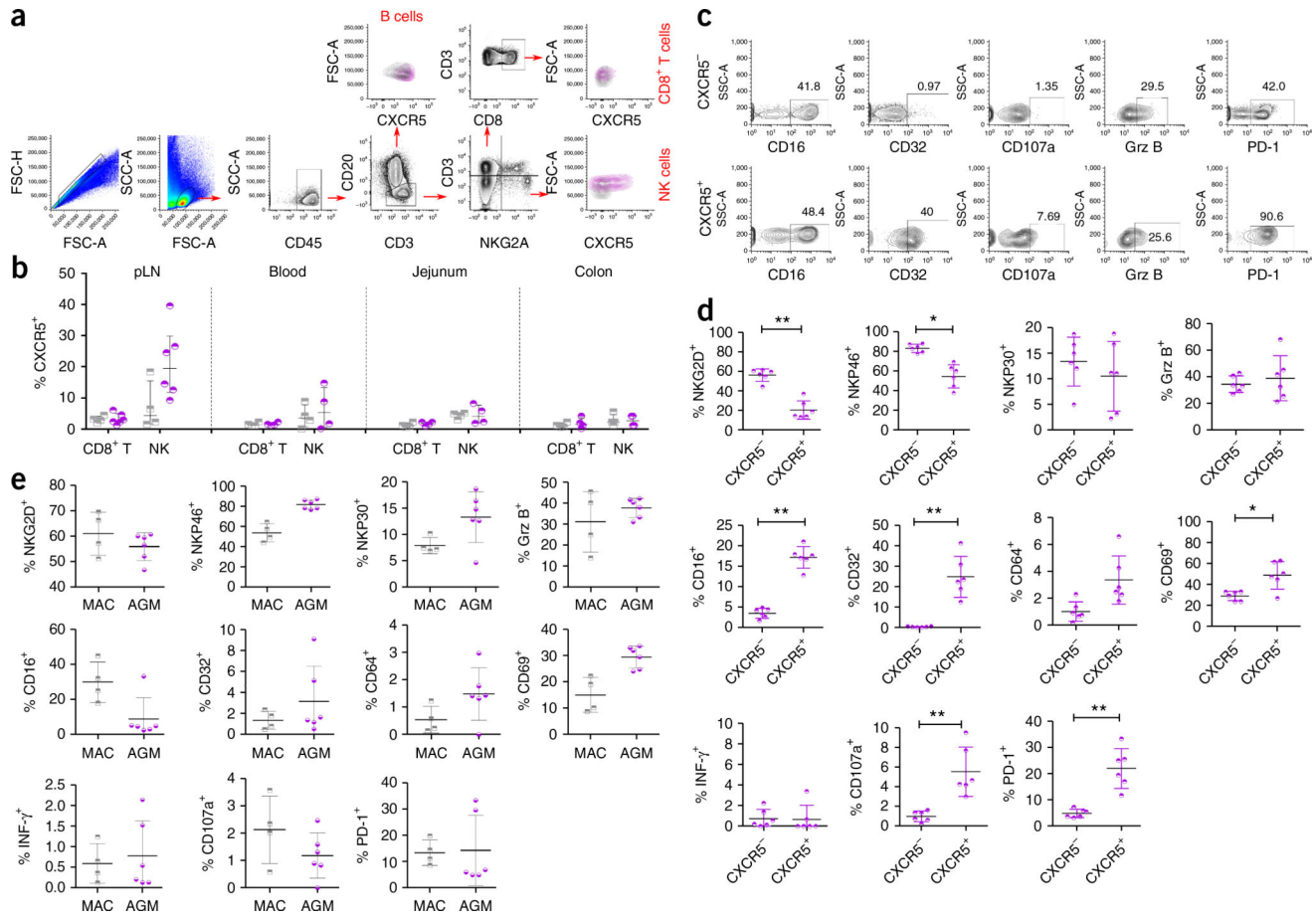

Figure 2.

CXCR5 expression on NK cells and phenotyping of CXCR5$^+$ NK cells in AGMs. CXCR5 was measured on cells from six chronically infected AGMs and six chronically infected macaques. (**a**) Gating strategy used to analyze CXCR5 expression on B cells, CD8$^+$ T cells and NK cells. Cells from macaques are plotted in gray, and those from AGMs are plotted in purple. Representative plots are shown. (**b**) Frequencies of CXCR5$^+$ cells for a given cell population in LNs from distinct tissues. pLN, peripheral lymph node. (**c**) Phenotypes of CXCR5$^-$ and CXCR5$^+$ NK cells from LNs in AGMs. A representative dot plot for one animal is shown. (**d**) Frequencies of CXCR5$^+$ and CXCR5$^-$ NK cells expressing given markers in AGM LN. (**e**) NK cell subset frequencies in LNs from AGMs and macaques. Individual values for AGMs are shown as purple circles and for macaques are shown as gray squares. The squared and circled regions in the dot plots represent those cells which have been considered for the subsequent analysis. The accompanying numbers indicate the percentage of these cells. A nonparametric Mann–Whitney *U*-test was applied in **d**. *$P <$ 0.05, **$P < 0.005$. Horizontal bars indicate median values, and error bars indicate standard deviation.

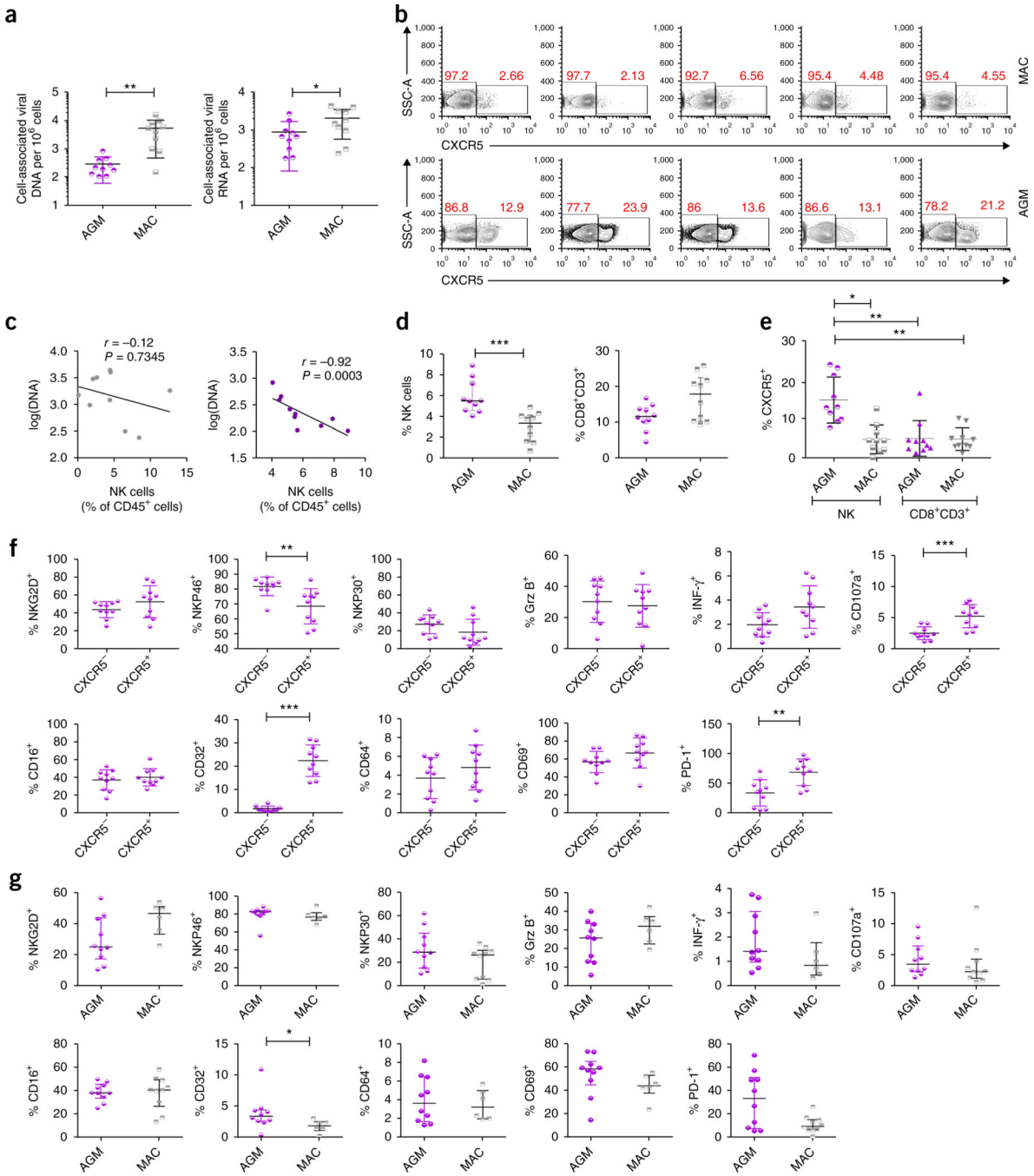

Figure 3.

Viral load and NK cells in spleen from chronically infected AGMs and macaques. Ten monkeys per species were analyzed. (**a**) Cell-associated SIV DNA and RNA levels in spleen. (**b**) CXCR5$^+$ NK cells. Representative dot plots for five of ten randomly chosen monkeys (alphabetical order) are shown. The left and right boxed areas represent the CXCR5$^-$ and CXCR5$^+$ NK cells, respectively. The accompanying numbers in red indicate the percentage of cells in each box. (**c**) Cell-associated viral DNA levels in spleen plotted against the frequencies of splenic NK cells in macaques (left) and AGMs (right). (**d**) Frequency of NK

cells among $CD45^+$ cells in spleen. (**e**) Frequencies of $CXCR5^+$ cells among NK and $CD8^+$ T cells in spleen. (**f**) Frequencies of $CXCR5^+$ and $CXCR5^-$ NK cells expressing given markers in spleen. (**g**) NK cell subsets in spleens from AGMs and macaques. Individual values for AGMs are shown as purple circles and for macaques are shown as gray squares. In **c**, a nonparametric Spearman's rank-order correlation was performed to determine the relationship between log(SIV DNA) and NK cell frequency for each species. For all panels except **c**, a nonparametric Mann–Whitney *U*-test was applied. $*P < 0.05$, $**P < 0.005$, $***P < 0.0005$. Horizontal bars indicate median values, and error bars indicate standard deviation.

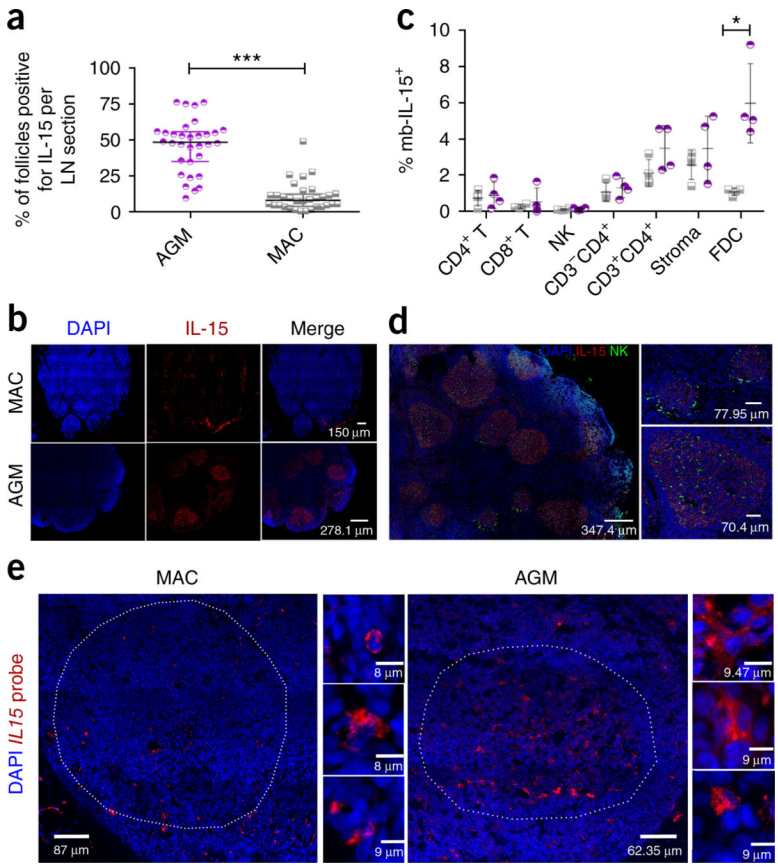

Figure 4.

IL-15 expression in lymph nodes during SIV infection in AGMs and macaques. LNs from six chronically infected AGMs and six chronically infected macaques were analyzed. (**a**) Percentage of follicles with at east one IL-15^{+} cell per analyzed LN section. A total of ten LN sections per animal were counted. (**b**) Confocal images of LN sections stained for IL-15 (red) and total nucleus (blue). Images present the distribution of IL-15^{+} cells for each species. (**c**) Frequencies of cells positive for both IL-15 and IL-15Rα among distinct subpopulations of stromal (CD45^{-}) and hematopoietic (CD45^{+}) cells. AGM, purple circles; macaque, gray squares. (**d**) Confocal images of LN sections stained for NK cells (green), IL-15 (red) and nucleus (blue), showing the spatial association between IL-15 and NK cells. The images on the right are higher-magnification images of AGM follicles with typical NK cell distribution, i.e., within and surrounding IL-15-positive follicles, during SIVagm infection. (**e**) Confocal images of LN sections hybridized with an *IL15* RNA probe (red) and stained with DAPI (blue). Circled areas represent B cell follicle limits. Images to the right show representative examples of the shape of *IL15*-mRNA-positive cells. In **a** and **c**, nonparametric Mann–Whitney *U*-tests were applied. *$P < 0.05$, ***$P < 0.0005$. Median and interquartile range are shown.

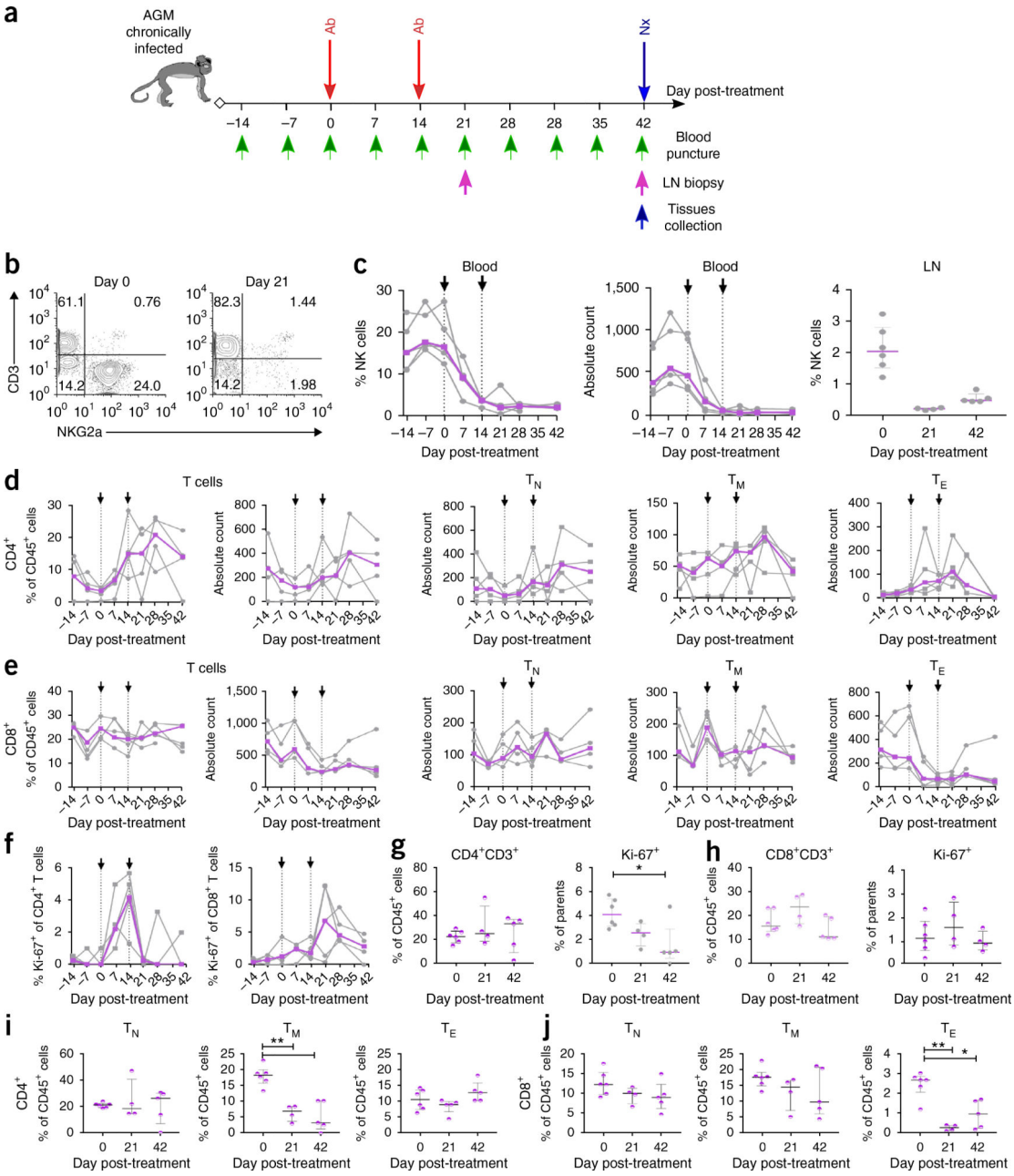

Figure 5.

Anti-IL-15 administration results in near-complete NK cell depletion in AGMs. (**a**) Schematic representation of the anti-IL-15 treatment schedule used in this study. Five chronically infected AGMs received 20 mg per kg body weight (mg/kg) of anti-IL-15 monoclonal antibody (Ab) on day 0 and 10 mg/kg on day 14. Red arrows show the days when anti-IL-15 monoclonal antibody was administered. The blue arrow indicates the day of necropsy (Nx). (**b**) Dot plots showing NK cells ($CD3^{-}NKG2A^{+}$) in peripheral blood from one representative AGM before and after anti-IL-15 administration. The numbers represent the percentages of NK cells among $CD45^{+}CD20^{-}$ cells. (**c**) Follow-up of NK cells in blood and LN. Blood was analyzed for five monkeys. LNs were available for four and five

monkeys at day 21 and day 42 post-treatment, respectively. For blood, gray and purple lines represent the trajectories for individual animals and the median values for all monkeys, respectively. For statistical analyses, mean values for the three preinfection time points were used for **c**–**f**. (**d**) Follow-up of $CD4^+$ T cells and subpopulations of $CD4^+$ T cells in blood during anti-IL-15 treatment. T_N, naive T cells; T_M, central memory T cells; T_E, effector memory T cells. (**e**) Follow-up of $CD8^+$ T cells and subpopulations of $CD8^+$ T cells in blood during anti-IL-15 treatment. (**f**) $CD4^+$ T cells and $CD8^+$ T cells positive for Ki-67 in blood. In **c**–**f**, black arrows indicate the days when anti-IL-15 monoclonal antibody was administered. (**g**) $CD4^+$ T cells in LN. (**h**) $CD8^+$ T cells in LN. In **g** and **h**, parent cells are $CD4^+CD3^+$ and $CD8^+CD3^+$, respectively. (**i**) $CD4^+$ T cell subpopulations in LN. (**j**) $CD8^+$ T cell subpopulations in LN. Median values and interquartile range are shown for **g**–**j**. Each dot represents the value for an individual animal. Nonparametric Mann–Whitney *U*-tests were applied. $*P < 0.05$, $**P < 0.005$.

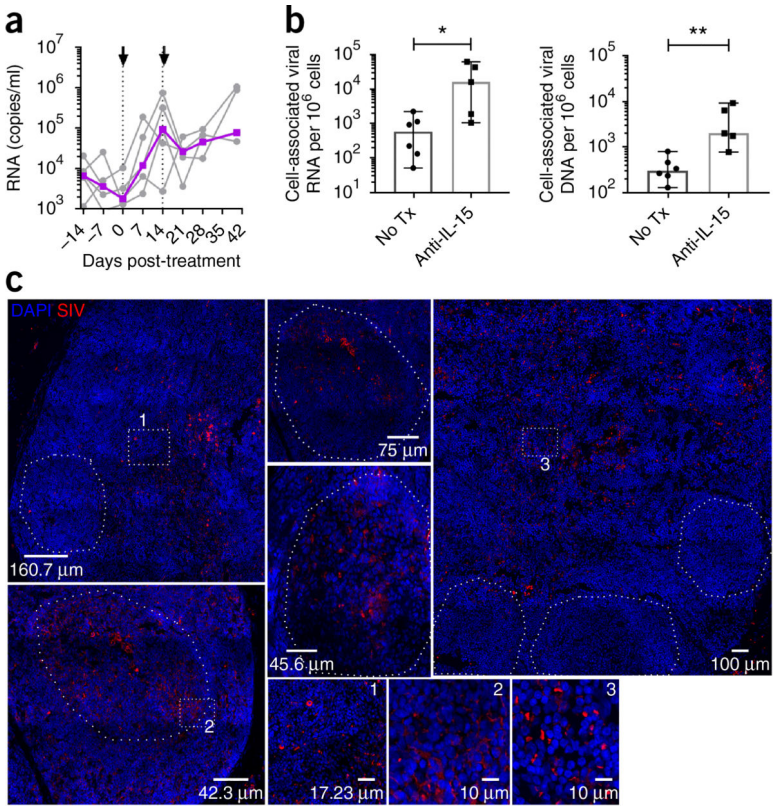

Figure 6.

NK cell depletion results in increases in SIV RNA, SIV DNA and productively infected cells in lymph nodes. (**a**) Quantification of SIVagm. sab_{92018} RNA in plasma by qRT–PCR in five chronically infected AGMs (the same as in Fig. 5) before and after anti-IL-15 administration. The gray line represents the viremia levels in individual monkeys over time, and the purple line represents the median viremia. The black arrows show the days of anti-IL-15 administration. (**b**) Quantification of the cell-associated SIV RNA and DNA levels in LN. The LNs of six monkeys without treatment were compared to LNs from five anti-IL-15-treated monkeys. Each dot represents an individual animal. Tx, anti-IL-15 treatment. (**c**) Virus-producing cells (SIV RNA; red) in the LNs of NK cell–depleted AGMs. Representative images are shown of an inguinal LN for five different monkeys, with one image for each of the five anti-IL-15-treated monkeys. The panels numbered 1, 2 and 3 correspond to magnified views of the labeled squared regions. Follicles are enclosed by the dashed white lines. Nonparametric Mann–Whitney *U*-tests were applied in **b** in each graph, Horizontal bars indicate median values with error bars indicating standard deviation (s.d). $*P < 0.05$, $**P < 0.005$. Horizontal bars indicate median values, and error bars indicate standard deviation.